ANALYSIS OF GAS-DYNAMIC PROCESSES AND DEVELOPMENT OF MODEL OF FLOWS IN HYPERSONIC SHOCK TUBE

V.V. Kuzenov, **M.A. Kotov**

Ishlinskii Institute for Problems in Mechanics of the RAS,
Moscow, Russian Federation
e-mail: kuzenov@ipmnet.ru; mikhail_kotov88@mail.ru

The paper considers the simplified one-dimensional mathematical models of the processes, which describe both formation and propagation of shock waves, rarefaction waves, and contact discontinuities in shock tubes. These models are based on the quasi-one-dimensional equations of radiation gas dynamics. Experimental and theoretical studies of both the formation and propagation of shock waves, rarefaction waves and contact discontinuities using shock tubes have always been of significant interest and they are currently being developed. It results from the fact that the shock tubes are the most convenient tool of laboratory research in such contemporary fields of modern science and technology as aerophysics and chemical kinetics, gas dynamics and molecular physics. The flows of a multicomponent gas proves to be important for many modern technological and power facilities as well as in hypersonic aircraft. The multicomponent gas undergoes chemical conversions, oscillatory, and electron excitation. A relatively simple instrument for creating non-equilibrium processes in the gases is a shock wave propagating in a tube of a circular or rectangular cross-section. This cross-section geometry allows simplifying the gas-dynamic flow pattern in the working section.

Keywords: shock tube, gas dynamics equations, nonlinear quasimonotonous compact difference scheme, Runge–Kutta multistep method

The problem statement. The aim of the paper is to examine the processes of formation and propagation of shock waves (SW), rarefaction waves and contact discontinuities in shock tubes using simplified one-dimensional mathematical models.

One of the important tasks is to develop numerical methods and a computational model code to describe unsteady one-dimensional radiation-magnetogasodynamic processes in different types of shock tubes.

Description of processes occurring in shock tubes. The shock tubes that generate shock waves have the following principle of operation (Fig. 1): the shock wave is generated in the tube containing a test (driven) gas when a "piston" of some kind is moving at a hypersonic speed. The shock tube, in which a compressed air is used for generating shock waves, operates in the most effective way when the ratio of the velocity of a sound in the working gas (C_R — driver gas) to the velocity of sound in the test gas (C_{St} — driven gas) is sufficiently high ($C_R/C_{St} \gg 1$). The heating of the driver gas in a shock tube with an electric discharge, solid or gaseous substances may be accompanied by a remarkable increase of the ratio mentioned above. This is related to the fact that the gas temperature can increase from 2 κK (without gas heating) up to 20 κK (with gas heating), which results in the

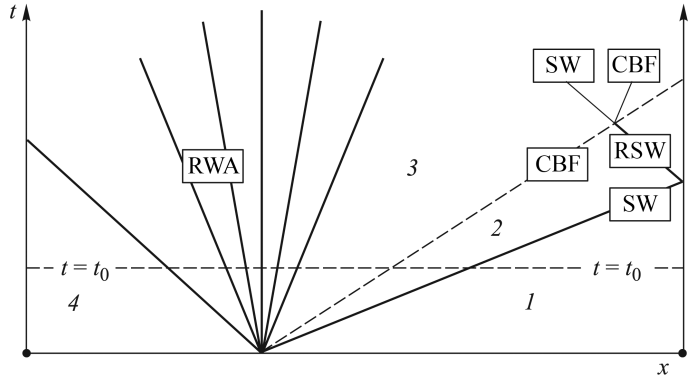

Fig. 1. Diagram of interaction processes of shock waves, rarefaction waves and contact discontinuities in the one-diaphragm shock tube after the rupture of the diaphragm:
SW — shock wave front; CBF — contact boundary front; RWA — rarefaction wave area; RSW — reflected shock wave front

significant (in this case about three times higher) increase of the sound velocity in the driver gas (C_R) and the proportional increase of the ratio C_R/C_{St}.

In the shock tubes, the shock wave front surface that is generated in the test (driven) gas is close to plane and the gas flow in the working path of the shock tube can be considered one-dimensional in a first approximation. In the simpliest shock tube, the system of waves mentioned above is generated after the rupture of the diaphragm (made of metal foil or lavsan film) separating the low pressure chamber containing the low pressure test gas (about 0.1. . .0.01 atm), from the high pressure chamber containing the compressed gas (with pressure from several to hundreds atmospheres).

One of the important tasks in the theory of the shock tube is to establish mathematical relationships between physical values, which define the state of gas in a shock tube at the initial time, and the parameters of the system of mentioned waves at any optional time.

These relationships can be found using methods of mathematical modeling, which (in case of using high-accuracy computational methods) reveal the detailed structure of the gas flow that undergoes physical-chemical transformations, if strong and weak interacting discontinuities are present in the flow area.

However, despite the development of multidimensional computational techniques, one-dimensional mathematical models retain their practical value, in particular, they allow verifying the models describing non-equilibrium chemical transformations by the comparison of numerical and experimental results.

The one-dimensional mathematical model of a gas flow in the path of the shock tube can be developed if a number of simplifying assumptions is

introduced. This elementary theory of the shock tube can be described by a simplified scheme of the physical processes (the assumptions are listed below). This simplified physical picture of the thermophysical processes in a shock tube is as follows:

— after the forced rupture of the diaphragm (using a special technical device), the driver gas in the high pressure chamber expands (compressing the test gas) into the low pressure chamber filled with the test (driven) gas under low pressure.

— in the low pressure chamber, a generated shock wave is propagating in the test gas, and in the high pressure chamber a rarefaction wave is propagating in the expanding driver gas;

— after the shock wave has reached the end of the pipe, it is reflected and comes back towards the driver gas;

— then this reflected shock wave is interacting with the contact discontinuity that separates the driver gas and the test gas, which results in shock wave partial reflection (in the form of a shock wave or a rarefaction wave (the criterion identifying these two cases is given below) and partial refraction and moving (in the form of a shock wave) into the compressed layer of the driver gas.

Here the following should be noted:

• if the shock wave interacting with the contact discontinuity escapes from a denser medium into the less dense one, it is reflected from the contact discontinuity in the form of a rarefaction waves fan;

• if the shock wave escapes from a less dense medium into the denser one, it is reflected in the form of a shock wave.

The course of flow in the aerodynamic shock tube can be conveniently represented in the form of the so-called $x{-}t$-diagram (Fig. 1). In $x{-}t$-diagram, area *1* corresponds to the unperturbed initial state of the test (driven or accelerated) gas, area *2* corresponds to the gas compressed in the shock wave, areas *3* and *4* are the areas of gas "piston" and unperturbed initial state of the gas in the high presure chamber before the rarefaction wave arrival.

The surface denoted by K and separating (between areas *2* and *3*) the test (driven or accelerated) gas and the driver (accelerating) gas is referred to as a contact surface (CS) or interface. The gas pressures and the flow velocities on either side of the CS are equal $(p_2 = p_3,\ u_2 = u_3)$. In the subsequent instant of time, the shock wave and the rarefaction wave are reflected from the end walls of the shock tube and begin to interact with each other.

Experimental and theoretical research into generation and propagation of the shock waves, rarefaction waves and contact discontinuities in

the shock tube shows that there are deviations from an idealized one-dimensional gas flow. For example, in most studied cases, the speed of the shock wave and the contact surface speed are practically equal. This similarity of the speed values of the CS and the shock wave results from the CS acceleration, which, in its turn, is associated with the formation of a boundary layer (which decelerates the shock wave) on the walls of the aerodynamic shock tubes.

This effect can be explained as follows: the speed of the shock wave front appears to be lower and the CS speed to be higher than the one-dimensional theory predicts, which in its turn, is connected with the fact that the gas piston (the CS plays its role) pushing the shock wave is not completely impenetrable: the mass flux discharging into the front expands from the shock-compressed area into the wall boundary layer, and thus the mass concentrated between the shock wave front and the contact surface remains constant.

This effect is the most appreciable when condition $\frac{L}{R} \gg 1$ is satisfied (where L, R are the shock tube length and the radius), as well as when the initial pressure of the test (driven or accelerated) gas decreases [1]. In this case, the dynamic boundary layer "displaces" most effectively the gas flow moving along the tube axis from the area which is adjacent to the tube wall. This effect of flow displacement can be taken into account (in a first approximation) by the use of boundary layer approximate equations and gas dynamics quasi-one-dimensional equations.

An important factor, which misrepresent the one-dimensional gas flow in a shock tube, is the duration of the diaphragm rupture (the time of the diaphragm opening that depends on the material of the diaphragm and the pressure value in the high-pressure chamber); it ranges from 100 to 1000 μs. The gas flow pattern after the rupture of the diaphragm central part corresponds to the discharge of the pulse gas jet into the low pressure area. The disturbances (of the shock wave or of the compression wave) caused by the expanding jet in the test (driven or accelerated) gas, are reflected from the walls of the shock tube and create spatial stream uniformities in the flow structure. These uniformities result in deviation from the idealized one-dimensional gas flow pattern.

It is also important that the contact boundary surface (separating the driver gas from the test gas) is unstable and in the course of time acquires an irregular spatial (bell-shaped) shape. The gases remaining on different sides of the contact boundary may mix, which results in the nonuniformity (non-one-dimensionality) of a gas flow stream in the shock tube.

It should be noted that the proposed computing algorithms for the numerical modeling of aerothermophysical characteristics of the shock

tubes should be supported by the following: methodical calculations, accuracy control, comparison of numerical results with analytical solutions and published designed and experimental results.

One-dimensional numerical method of the medium parameters computing in the working section of a shock tube. Despite the one-dimensional nature of the task relating to the multiple pass calculation, reflection (from end faces of the shock tube) and interaction of previously described system of waves, it steps up the demands for the numerical method used in addressing it. First of all the design model must have the improved dispersion and dissipation properties; it must be cost-effective, algorithmically simple, and monotonous; it must approximate smooth solutions with the highest order of accuracy.

These requirements can be satisfied by using a numerical solution method for the quasi-one-dimensional synthermal one-fluid equations of gas dynamics, which is based on the subincremental method. In this case it consists of two steps [2]. The systems of equations mentioned above can be solved using a version of the nonlinear quasimonotonous compact difference scheme of the higher order of accuracy, developed by the authors. Let us describe the ways to find the numerical solution of these fractional steps.

The first fractional step involves gas-dynamic processes (the hyperbolic part of the equations set in question agrees with these processes) that occur in the shock tube after the rupture of the diaphragm, which separates the driver gas from the test (driven) gas; the second fractional step involves the quasi-one-dimensional geometry of the facility.

Mathematical formulation of the first fractional step and the solution to the hyperbolic part of the equations set are based on the divergence form and can be formulated by the following:

$$\frac{\partial \vec{U}}{\partial t} + \frac{\partial F\left(\vec{U}\right)}{\partial \xi} = \vec{F}_2,\ F_\rho = -\rho v \frac{d\ln F}{dz};$$

$$F_{\rho v} = -\rho v^2 \frac{d\ln F}{dz},\ F_E = -\left(\rho E v + vP\right)\frac{d\ln F}{dz};$$

or

$$\frac{\partial \vec{U}}{\partial t} = L\left(U\right),\ L = -\frac{\partial F\left(\vec{U}\right)}{\partial \xi} + \vec{F}_2;$$

here the parameter ξ can take one of the values from the value set (r, z), the solution vector is $\vec{U} = (\rho, \rho u_\xi, \rho E)^{\mathrm{T}}$, the flow variable vector can be written as $F\left(\vec{U}\right) = \left(\rho u_\xi, \rho u_\xi^2 + P,\ \rho E u_\xi + P u_\xi\right)^{\mathrm{T}}$, and the right part vector is presented as $\vec{F}_2 = (F_\rho, F_{\rho u}, F_E)^{\mathrm{T}}$.

It should be noted that the differential equations sets mentioned above and related to the time variable t, are the sets of conventional differential equiations of the first order, which can be solved using a vector version of the Runge-Kutta multistep method (in the present paper, a four-step version of the method [3] is used, which has the fourth order of approximation relative to time t).

We bring the vector version of the Euler's equations set to a normal form with a time derivative defined in the left part $\dfrac{\partial \vec{U}_i}{\partial t}$:

$$\frac{\partial \vec{U}_i}{\partial t} = L\left(\vec{U}_i\right),$$

where L is the right part of the Euler's equations set that does not contain time derivatives. To a first approximation we use the solution obtained at the previous time step. Then the four-step version of Runge-Kutta method can be implemented in the form of the following sequence of steps:

$$\vec{U}_i^{(1)} = \left[\vec{U}_i^{(0)} + \frac{\Delta t}{4} L\left(\vec{U}_i^{(0)}\right)\right],$$

$$\vec{U}_i^{(2)} = \left[\vec{U}_i^{(0)} + \frac{\Delta t}{3} L\left(\vec{U}_i^{(1)}\right)\right],$$

$$\vec{U}_i^{(3)} = \left[\vec{U}_i^{(0)} + \frac{\Delta t}{2} L\left(\vec{U}_i^{(2)}\right)\right],$$

$$\vec{U}_i^{(4)} = \left[\vec{U}_i^{(0)} + \Delta t L\left(\vec{U}_i^{(3)}\right)\right].$$

It is known that this way of searching for a solution $\vec{U}_i$ relative to t, solves one of the problems of the Euler's equations numerical solution , i.e. the need to ensure the positivity of the required functions (if at the time instant t^n the solution is positive, it remains positive at the time instant t^{n+1} as well).

The rise of the approximation order relative to time variable t of the Euler's equations system numerical solution to the fourth order $O\left(\Delta t^4\right)$ and higher is also possible if the sequence of meshes by time variable t and extrapolation by limit offered by Richardson will be used. The Richardson extrapolation has the following specific features:

- the possibility to use the simpliest approximations of differential problems;
- the uniformity of algorithms implementation on the sequence of meshes with different parameters of approximation;
- the simplicity of the algorithm realization in general.

Let us take the solution to the problem in question obtained by intergating (with the second order of approximation $O(\Delta t^2)$) relative to time t with increment Δt at the time instant $\widehat{t} = t + \Delta t$, which we denote as $(\rho, u, v, P)|_{t+\Delta t}$, and also the solution (with the second order of approximation $O(\Delta t^2)$), denoted as $(\rho, u, v, P)|_{t+\Delta t/2}$, obtained by using two time increments (each increment is equal to $\Delta t/2$) before the time instant $\widehat{t} = t + \Delta t$.

Then the linear combination:

$$\overline{\overline{(\rho, u, v, P)|^{\widehat{t}}_{t+\Delta t}}} = \frac{4}{3}(\rho, u, v, P)|^{\widehat{t}}_{t+\Delta t/2} - \frac{1}{3}(\rho, u, v, P)|^{\widehat{t}}_{t+\Delta t}$$

brings the exact solution nearer to the approximation of the fourth order relative to time variable $O(\Delta t^4)$ [4].

To bring the exact solution nearer to the sixth or eighth order of approximation relative to time variable, the formulas [5] should be used:

$$\overline{\overline{(\rho, u, v, P)|^{\widehat{t}}_{t+\Delta t}}} = \frac{32}{21}(\rho, u, v, P)|^{\widehat{t}}_{t+\Delta t/4} - \\ -\frac{4}{7}(\rho, u, v, P)|^{\widehat{t}}_{t+\Delta t/2} + \frac{1}{21}(\rho, u, v, P)|^{\widehat{t}}_{t+\Delta t};$$

$$\overline{\overline{(\rho, u, v, P)|^{\widehat{t}}_{t+\Delta t}}} = \frac{512}{315}(\rho, u, v, P)|^{\widehat{t}}_{t+\Delta t/8} - \\ -\frac{32}{45}(\rho, u, v, P)|^{\widehat{t}}_{t+\Delta t/4} + \frac{4}{45}(\rho, u, v, P)|^{\widehat{t}}_{t+\Delta t/2} - \frac{1}{315}(\rho, u, v, P)|^{\widehat{t}}_{t+\Delta t}.$$

At the first fractional step, the following divergent form of Euler's equiations is used:

$$\frac{\partial \rho}{\partial t} + \frac{\partial \rho u_\xi}{\partial \xi} = F_\rho, \frac{\partial (\rho u_\xi)}{\partial t} + \frac{\partial \left(\rho u_\xi^2 + P\right)}{\partial \xi} = F_{\rho u},$$

$$\frac{\partial (\rho E)}{\partial t} + \frac{\partial (\rho E u_\xi + P u_\xi)}{\partial \xi} = F_E,$$

$$\frac{\partial \vec{U}}{\partial t} + \frac{\partial F\left(\vec{U}\right)}{\partial \xi} = \vec{F}_2,$$

where $u_\xi = (u, v)$, parameter ξ can take one of the set of values (r, z), the solution vector is $\vec{U} = (\rho, \rho u_\xi, \rho E)^{\mathrm{T}}$, the vector of the flow variable will be written as $F\left(\vec{U}\right) = \left(\rho u_\xi, \rho u_\xi^2 + P, \rho E u_\xi + P u_\xi\right)^{\mathrm{T}}$, and the right part vector will be given as $\vec{F}_2 = (F_\rho, F_{\rho u}, F_E)^{\mathrm{T}}$. Here (for the time fractional step $t \in [t, t + \Delta t/2]$), the non-linear quasi-monotonous conpact difference scheme of the higher order of accuracy is used, which in the space-smooth

part of the numerical solution permits to acheve the seventh order of accuracy:

$$\frac{\partial \vec{U}_i}{\partial t} + \frac{F\left(\vec{U}_{i+1/2}\right) - F\left(\vec{U}_{i-1/2}\right)}{\Delta\xi} = \vec{F}_2.$$

Gas-dynamic parameters U_i^{n+1}, U_i^n are related to the centers of design meshes, while the flows $F_{i\pm1/2}^n, G_i^n$ are to be determined on the surface of these meshes. To rise the order of the approximation of the difference scheme, one should retrieve the gas-dynamics parameters $Y_{i\pm1/2}^{R,L}, Y_i^{R,L}$ on the right (index R) and on the left (index L) from the boundaries of the design meshes. Then any function being retrieved $Y(x), [x = \{\xi\}]$, $\xi \in [-\frac{\Delta_\xi}{2}, \frac{\Delta_\xi}{2}]$, can be represented by piecewise-polynomial distributions:

$$Y(\xi) = Y_i + \left\{ \left(\frac{\partial Y}{\partial \xi}\right)_i [\xi - \xi_i] + \frac{1}{2!}\left(\frac{\partial^2 Y}{\partial \xi^2}\right)_i [\xi - \xi_i]^2 - \right.$$
$$- \frac{2}{3!}\left(\frac{\partial^2 Y}{\partial \xi^2}\right)_i \left[\frac{\Delta_\xi}{2}\right]^3 + \frac{1}{3!}\left(\frac{\partial^3 Y}{\partial \xi^3}\right)_i [\xi - \xi_i]^3 + \frac{1}{4!}\left(\frac{\partial^4 Y}{\partial \xi^4}\right)_i [\xi - \xi_i]^4 -$$
$$- \frac{2}{5!}\left(\frac{\partial^4 Y}{\partial \xi^4}\right)_i \left[\frac{\Delta_\xi}{2}\right]^5 + \frac{1}{5!}\left(\frac{\partial^5 Y}{\partial \xi^5}\right)_i [\xi - \xi_i]^5 +$$
$$\left. + \frac{1}{6!}\left(\frac{\partial^6 Y}{\partial \xi^6}\right)_i [\xi - \xi_i]^6 - \frac{2}{7!}\left(\frac{\partial^4 Y}{\partial \xi^4}\right)_i \left[\frac{\Delta_\xi}{2}\right]^7 \right\},$$

where $Y_{i+1/2}^R = Y\left(\xi = \frac{\Delta_\xi}{2}\right)$, $Y_{i-1/2}^L = Y\left(\xi = -\frac{\Delta_\xi}{2}\right)$, etc. Note, that the formula data satisfy the balance relations: $Y_i = \frac{1}{\Delta_\xi} \int\limits_{\xi_{i-1/2}}^{\xi_{i+1/2}} (\xi) d\xi$.

These piecewise-polynomial distributions should be limited (to bring them to the monotonous form) by a function-limiter $\varphi(Y)$ [6]:

$$\varphi(Y_i) = \min\left(1, \frac{|Y_i - \max(Y_k)|}{\left|Y_i - \max\left(Y_{k-1/2}, Y_{k+1/2}\right)\right|}, \frac{|Y_i - \min(Y_k)|}{\left|Y_i - \min\left(Y_{k-1/2}, Y_{k+1/2}\right)\right|}\right),$$

where $k = i-2, i-1, i+1, i+2$; i.e.,

$$Y(\xi) = Y_i + \varphi(Y_i) \left\{ \left(\frac{\partial Y}{\partial \xi}\right)_i [\xi - \xi_i] + \right.$$
$$+ \frac{1}{2!}\left(\frac{\partial^2 Y}{\partial \xi^2}\right)_i [\xi - \xi_i]^2 - \frac{2}{3!}\left(\frac{\partial^2 Y}{\partial \xi^2}\right)_i \left[\frac{\Delta_\xi}{2}\right]^3 +$$
$$+ \frac{1}{3!}\left(\frac{\partial^3 Y}{\partial \xi^3}\right)_i [\xi - \xi_i]^3 + \frac{1}{4!}\left(\frac{\partial^4 Y}{\partial \xi^4}\right)_i [\xi - \xi_i]^4 - \frac{2}{5!}\left(\frac{\partial^4 Y}{\partial \xi^4}\right)_i \left[\frac{\Delta_\xi}{2}\right]^5 +$$
$$\left. + \frac{1}{5!}\left(\frac{\partial^5 Y}{\partial \xi^5}\right)_i [\xi - \xi_i]^5 + \frac{1}{6!}\left(\frac{\partial^6 Y}{\partial \xi^6}\right)_i [\xi - \xi_i]^6 - \frac{2}{7!}\left(\frac{\partial^4 Y}{\partial \xi^4}\right)_i \left[\frac{\Delta_\xi}{2}\right]^7 \right\}.$$

The space variables $\left(\frac{\partial Y}{\partial \xi}\right)_{i,j}$ included in piecewise-polynomial distributions $Y(\xi)$ are computed as follows.

Firstly, for the discrete function Y_i we determine the approximate value F_i of the first partial derivative related to the space variable ξ with the eighth order of approximation.

There to, in each mesh with number i for each value to be retrieved $Y_{i,j}$ the index of non-monotony $Ind(Y)$ is to be computed:

$$Ind\,(Y)_i = \frac{\frac{1}{12}\left|-Y_{i+2,j}+16Y_{i+1,j}-30Y_{i,j}+16Y_{i-1,j}-Y_{i-2,j}\right|}{\left(\frac{1}{2}\left|-Y_{i+2,j}+4Y_{i+1,j}-3Y_{i,j}\right|+\frac{1}{2}\left|3Y_{i,j}-4Y_{i-1,j}+Y_{i-2,j}\right|+\theta\right)},$$

where θ is a small parameter.

Then we find the first derivative f by variable ξ according to the usual approximation formula of the second order of approximation and fulfil its "monotonous limitation" on the mesh:

$$\overline{Ind}\,(Y)_i = 1 \cdot Ind\,(Y)_i + 2 \cdot [1 - Ind\,(Y)_i];$$

$$f_i = \frac{Y_{i+1} - Y_{i-1}}{2\Delta},$$

$$\tilde{f}_i = \text{sign}(Y_{i+1} - Y_{i-1}) \min\left(\overline{Ind}\,(Y)_{i+1}\,|f_{i+1}|\,, |f_i|\,, \overline{Ind}\,(Y)_{i-1}\,|f_{i-1}|\right),$$

where Δ is a step of the space mesh in direction ξ. Then the approximate "monotonized" value of $\tilde{F}_i$ of the first partial derivative by the space variables ξ with the approximation error on the level of $F_i = \frac{\partial}{\partial \xi} + \frac{\Delta^6}{2100} + +O\left(\Delta^8\right)$ can be obtained by the formula (i.e., by the solution of the system of equations with the tridiagonal marix):

$$Q_i = \left(E + \frac{\Delta_2}{30}\right)\tilde{f}_i, \widetilde{F}_i = \left\{\left(E + \frac{\Delta_2}{6}\right)^{-1} Q_i\right\}_i;$$

$$\overline{F_i} = \text{sign}(Y_{i+1} - Y_{i-1}) \min\left(\left|\tilde{F}_{i+1}\right|, \left|\tilde{F}_i\right|, \left|\tilde{F}_{i-1}\right|\right);$$

$$F_i = \overline{F_i} + \text{sign}(Y_{i+1} - Y_{i-1}) \cdot [1 - Ind\,(Y)_i] \cdot \left|\widetilde{F}_i - \overline{F_i}\right|,$$

where $\Delta_0 f_i = f_{i+1} - f_{i-1}$, $\Delta_2 f_i = f_{i+1} - 2f_i + f_{i-1}$, E is a unit operator. Note, that the given formula is the symmetrical finite difference of the sixth order of approximation [7]. This form of computing of the first derivative F_i is used to form the edge conditions while obtaining the approximate "monotonized" value $\tilde{F}_i$ of the first partial derivative by the space variables

ξ with the approximation error on the level $F_i = \dfrac{\partial}{\partial\xi} + \dfrac{\Delta^8}{44100} + O\left(\Delta^{10}\right)$. In this case the computation should be done as follows (on the basis of of the equation system solution with pentadiagonal matrix [7]:

$$Q_i = \left(E + \frac{5\Delta_2}{42}\right)\tilde{f}_i,\ \widetilde{F}_i = \left\{\left(E + \frac{2\Delta_2}{7} + \frac{\Delta_2^2}{70}\right)^{-1} Q_i\right\}_i,$$

$$\overline{F_i} = \text{sign}(Y_{i+1} - Y_{i-1}) \min\left(\left|\tilde{F}_{i+1}\right|, \left|\tilde{F}_i\right|, \left|\tilde{F}_{i-1}\right|\right),$$

$$F_i = \overline{F_i} + \text{sign}(Y_{i+1} - Y_{i-1}) \cdot \left[1 - Ind\left(Y\right)_i\right] \cdot \left|\widetilde{F_i} - \overline{F_i}\right|.$$

In piecewise-polynomial distributions $Y(\xi)$ there are space derivatives of the second order $\left(\dfrac{\partial^2 Y}{\partial\xi^2}\right)_i = s_i$, which we further conventionally denote by s_i, and compute with the eighth order of accuracy [5]:

$$\frac{9}{38}\left(s_{i+1} + s_{i-1}\right) + s_i = -\frac{751}{342\Delta^2}Y_i + \frac{147}{152\Delta^2}\left(Y_{i+1} + Y_{i-1}\right) + \\ + \frac{51}{380\Delta^2}\left(Y_{i+2} + Y_{i-2}\right) - \frac{23}{6840\Delta^2}\left(Y_{i+3} + Y_{i-3}\right).$$

The space derivatives of the fourth $\left(\dfrac{\partial^4 Y}{\partial\xi^4}\right)_i = S_i^4$ and sixth $\left(\dfrac{\partial^6 Y}{\partial\xi^6}\right)_{i,j} = S_i^6$ orders can be obtained from the relations (i.e., by solving the equations systems with the tridiagonal matrix) [7]:

$$Q_i = \left(\frac{\Delta_2}{6}\right)\tilde{f}_i,\ \widetilde{S_i^4} = \left\{\left[E - \left(E + \frac{\Delta_2}{6}\right)^{-1}\right] Q\right\}_i;$$

$$S_i^4 = \Delta^4\left(\frac{\partial^4 Y}{\partial\xi^4}\right)_i - \frac{\Delta^8}{720} + O\left(\Delta^{10}\right);$$

$$Q_i = \left(\frac{\Delta_2}{12}\right)\tilde{S}_i^4,\ \widetilde{S_i^6} = \left\{\left[E - \left(E + \frac{\Delta_2}{12}\right)^{-1}\right] Q\right\}_i;$$

$$S_i = \Delta^6\left(\frac{\partial^6 Y}{\partial\xi^6}\right)_i - \frac{\Delta^{10}}{180} + O\left(\Delta^{12}\right).$$

The other derivatives included in the piecewise-polynomial distributions are determined by using variables $\left(\dfrac{\partial Y}{\partial\xi}\right)_i$ and $\left(\dfrac{\partial^2 Y}{\partial\xi^2}\right)_i$.

When the solution, which describes the displaceable part of the equation (i.e. $\frac{\partial Y}{\partial t} + V\frac{\partial Y}{\partial \xi} = 0$), is obtained, it is possible to approximate the "retrievable" distribution using the distribution $Y(\xi, \eta)$. Then it is possible to determine the average value $\tilde{Y}$ of function $Y(\xi)$ in different intervals: for the interval $\left[\xi_{i+1/2} - |V|\,t, \xi_{i+1/2}\right]$, if $V > 0$:

$$\tilde{Y}^L_{i+1/2}(|V|\,t) = \left(\frac{1}{\Psi}\right) \int\limits_{\xi_{i+1/2}-\Psi}^{\xi_{i+1/2}} Y(\xi)\,d\xi = Y_{i-1,j} + \\ + \varphi(Y_{i-1}) \left\{ -\frac{F_{2,i-1}\left(\tilde{\psi}\right)}{2!}\left[\frac{\Delta_\xi}{2}\right]^2 \left(\frac{\partial Y}{\partial \xi}\right)_{i-1} - \right. \\ -\frac{F_{3,i-1}\left(\tilde{\psi}\right)}{3!}\left[\frac{\Delta_\xi}{2}\right]^3 \left(\frac{\partial^2 Y}{\partial \xi^2}\right)_{i-1} - \frac{2}{3!}\left(\frac{\partial^2 Y}{\partial \xi^2}\right)_{i-1}\left[\frac{\Delta_\xi}{2}\right]^3 - \\ -\frac{F_{4,i-1}\left(\tilde{\psi}\right)}{4!}\left[\frac{\Delta_\xi}{2}\right]^4 \left(\frac{\partial^3 Y}{\partial \xi^3}\right)_{i-1} - \frac{F_{5,i-1}\left(\tilde{\psi}\right)}{5!}\left[\frac{\Delta_\xi}{2}\right]^5 \left(\frac{\partial^4 Y}{\partial \xi^4}\right)_{i-1,j} - \\ -\frac{2}{5!}\left(\frac{\partial^4 Y}{\partial \xi^4}\right)_{i-1}\left[\frac{\Delta_\xi}{2}\right]^5 - \frac{F_{6,i-1}\left(\tilde{\psi}\right)}{6!}\left[\frac{\Delta_\xi}{2}\right]^6 \left(\frac{\partial^5 Y}{\partial \xi^5}\right)_{i-1} - \\ \left. -\frac{F_{7,i-1}\left(\tilde{\psi}\right)}{7!}\left[\frac{\Delta_\xi}{2}\right]^7 \left(\frac{\partial^6 Y}{\partial \xi^6}\right)_{i-1} - \frac{2}{7!}\left(\frac{\partial^6 Y}{\partial \xi^6}\right)_{i-1}\left[\frac{\Delta_\xi}{2}\right]^7 \right\};$$

for the interval $\left[\xi_{i+1/2}, \xi_{i+1/2} + |V|\,t\right]$, if $V < 0$:

$$\tilde{Y}^R_{i+1/2}(|V|\,t) = \left(\frac{1}{\Psi}\right) \int\limits_{\xi_{i+1/2}}^{\xi_{i+1/2}+\Psi} Y(\xi)\,d\xi = Y_i + \\ + \varphi(Y_i) \left\{ \frac{F_{2,i}\left(\tilde{\psi}\right)}{2!}\left[-\frac{\Delta_\xi}{2}\right]^2 \left(\frac{\partial Y}{\partial \xi}\right)_i + \right. \\ +\frac{F_{3,i}\left(\tilde{\psi}\right)}{3!}\left[-\frac{\Delta_\xi}{2}\right]^3 \left(\frac{\partial^2 Y}{\partial \xi^2}\right)_i - \frac{2}{3!}\left(\frac{\partial^2 Y}{\partial \xi^2}\right)_i\left[\frac{\Delta_\xi}{2}\right]^3 + \\ +\frac{F_{4,i}\left(\tilde{\psi}\right)}{4!}\left[-\frac{\Delta_\xi}{2}\right]^4 \left(\frac{\partial^3 Y}{\partial \xi^3}\right)_i + \frac{F_{5,i}\left(\tilde{\psi}\right)}{5!}\left[-\frac{\Delta_\xi}{2}\right]^5 \left(\frac{\partial^4 Y}{\partial \xi^4}\right)_{i,j} -$$

$$- \frac{2}{5!}\left(\frac{\partial^4 Y}{\partial \xi^4}\right)_i \left[\frac{\Delta_\xi}{2}\right]^5 + \frac{F_{6,i}\left(\tilde{\psi}\right)}{6!}\left[-\frac{\Delta_\xi}{2}\right]^6 \left(\frac{\partial^5 Y}{\partial \xi^5}\right)_i - \\ + \frac{F_{7,i}\left(\tilde{\psi}\right)}{7!}\left[-\frac{\Delta_\xi}{2}\right]^7 \left(\frac{\partial^6 Y}{\partial \xi^6}\right)_i - \frac{2}{7!}\left(\frac{\partial^6 Y}{\partial \xi^6}\right)_i \left[\frac{\Delta_\xi}{2}\right]^7 \Bigg\},$$

where $\psi = |V|\, t$, $\tilde{\psi} = 2\,|V|\, t/\Delta_\xi = 2\psi/\Delta_\xi$).

Here, the following functions are introduced (symbol $\widetilde{\Psi}^m$, used in the following formulas, means exponentiation of the value $\widetilde{\Psi}$ to the m-th power):

$$F_2\left(\tilde{\psi}\right) = -2\widetilde{\Psi}^0 + \widetilde{\Psi}^1;$$

$$F_3\left(\tilde{\psi}\right) = -3\widetilde{\Psi}^0 + 3\widetilde{\Psi}^1 - \widetilde{\Psi}^2;$$

$$F_4\left(\tilde{\psi}\right) = -4\widetilde{\Psi}^0 + 6\widetilde{\Psi}^1 - 4\widetilde{\Psi}^2 + \widetilde{\Psi}^3;$$

$$F_5\left(\tilde{\psi}\right) = -5\widetilde{\Psi}^0 + 10\widetilde{\Psi}^1 - 10\widetilde{\Psi}^2 + 5\widetilde{\Psi}^3 - \widetilde{\Psi}^4;$$

$$F_6\left(\tilde{\psi}\right) = -6\widetilde{\Psi}^0 + 15\widetilde{\Psi}^1 - 20\widetilde{\Psi}^2 + 15\widetilde{\Psi}^3 - 6\widetilde{\Psi}^4 + \widetilde{\Psi}^5;$$

$$F_7\left(\tilde{\psi}\right) = -7\widetilde{\Psi}^0 + 21\widetilde{\Psi}^1 - 35\widetilde{\Psi}^2 + 35\widetilde{\Psi}^3 - 21\widetilde{\Psi}^4 + 7\widetilde{\Psi}^5 - \widetilde{\Psi}^6.$$

When the solution describing the displaceable part of the equiation (i.e. $\dfrac{\partial c}{\partial t} + V\dfrac{\partial c}{\partial x} = 0$) is obtained, it is also possible to retrive the distribution by the piecewise-polynomial distributions $Y(x)$, $[x = \{\xi\}]$, $\xi \in \left[-\dfrac{\Delta_\xi}{2}, \dfrac{\Delta_\xi}{2}\right]$, approximate by parabola $q(x) = q_i^L + \xi\left(\Delta q_i + q_i^6\,(1-\xi)\right)$, where $\xi = \left(x - x_{i-1/2}\right)h^{-1}$, $\Delta q_i = q_i^R - q_i^L$, $q_i^6 = 6\left(q_i - (1/2)\left(q_i^L + q_i^R\right)\right)$, $q_i^L = \tilde{Y}_{i+1/2}^L\left(|V|\, t\right)$, $q_i^R = \tilde{Y}_{i+1/2}^R\left(|V|\, t\right)$.

Then, the average value $\tilde{q}$ of the function $q(x)$ can be found in separate intervals:

- for interval $\left[x_{i+1/2} - |V|\, t, x_{i+1/2}\right]$, if $V > 0$:

$$\tilde{q}_{i+1/2}^L(y) = q_i^R - (1/2)\, yh^{-1}\left(\Delta q_i - q_i^6\left(1 - (2/3)\, yh^{-1}\right)\right), \quad y = Vt;$$

- for interval $\left[x_{i+1/2}, x_{i+1/2} + |V|\, t\right]$, if $V < 0$:

$$\tilde{q}_{i+1/2}^R(y) = q_{i+1}^L + (1/2)\, yh^{-1}\left(\Delta q_{i+1} + q_{i+1}^6\left(1 - (2/3)\, yh^{-1}\right)\right), \; y = -Vt.$$

Note, that distribution $q(x)$ is connected with the mentioned above distribution Y by formulae: $\Delta q_i = \left(\dfrac{\partial Y}{\partial \xi}\right)_i$, $q_i^6 = -\dfrac{1}{2}\left(\dfrac{\partial^2 Y}{\partial \xi^2}\right)_i$.

This results in the numerical method of solving the quasi-one-dimensional equations of gas-dynamics (physically specified well), underlaid by the predictor-corrector method and a variant of the non-linear quasi-monotonous compact difference scheme of the higher order of accuracy. In this case, for the "predictor" stage, the system of Euler's quasi-one-dimensional equations is used in a general non-divergent characteristic form, in which the unknown values are written relative to the Riemann quasiinvariants. At the "corrector" stage, the divergent form of Euler's quasi-one-dimensional equations is used.

Time increment Δt, necessary for integrating the difference scheme given above, is selected from the conditions of satisfying the Courant-Friedrichs-Lewy stability criterion.

To approximate the second derivatives that are included into the "viscous" part of the equations set of the dynamic and thermal boundary layer, we used the finite-difference presentation of $(\mu f)'_z$ the variables on the mesh introduced earlier by the following formulae [7]:

$$(\mu f)'_z \approx \frac{\left[\mu_{i-1} f'_{i-1} + 8\left(\mu_{i+1/2} f'_{i+1/2} - \mu_{i-1/2} f'_{i-1/2}\right) - \mu_{i+1} f'_{i+1}\right]}{6\Delta};$$

$$\mu_{i\pm 1/2} = \frac{\left[\mu_{i\pm 2} + 9\left(\mu_i + \mu_{i\pm 1}\right) - \mu_{i\mp 1}\right]}{16};$$

$$f'_{i\pm 1/2} \approx \frac{\left[27\left(\mp f_i \pm f_{i\pm 1}\right) \pm \left(f_{i\mp 1} \mp f_{i\pm 2}\right)\right]}{12\Delta};$$

$$f'_{i\pm 1/2} \approx \frac{\left[\mp f_{i\mp 2} \pm 6 f_{i\mp 1} \mp 18 f_i \pm 10 f_{i\pm 1} \pm 3 f_{i\pm 2}\right]}{12\Delta}.$$

Mixed derivatives $\dfrac{\partial}{\partial x}\left[\mu \dfrac{\partial f}{\partial y}\right]_{i,j}$ have been approximated by the known central differencies of the fourth order (or with the formulas given): $(\mu f)'_z \approx \dfrac{\left[f_{i-2} + 8\left(f_{i+1} - f_{i-1}\right) - f_{i+2}\right]}{12\Delta}$. The approximation effectiveness of using "viscous" members of the boundary layer of high order accuracy operators is particularly noticeable in the tasks relating to the computation of the aerodynamic shock tubes. Let us use the displacement operator $T_m u_j = u_{j+m} = u\left(z_j + m\Delta\right)$ and the symbol of unit operator $E = T_0$ to determine the derivatives $\left.\dfrac{\partial v}{\partial r}\right|_{r=R}$, $\left.\dfrac{\partial \zeta}{\partial r}\right|_{r=R-\delta}$ at the boundary of the design area:

$$u'|_{r=R} = \frac{1}{60\Delta}[-12T_{-5} + 75T_{-4} -$$
$$-200T_{-3} + 300T_{-2} - 300T_{-1} + 137E] + \frac{\Delta^5}{6} u^{\mathrm{VI}};$$

$$u'|_{r=R} = \frac{1}{60\Delta}[10T_{-6} - 72T_{-5} +$$
$$+225T_{-4} - 400T_{-3} + 450T_{-2} - 360T_{-1} + 147E] + \frac{\Delta^6}{7}u^{\text{VII}};$$

$$u'|_{r=R-\delta} = \frac{1}{60\Delta}\,[12T_5 - 75T_4 + 200T_3 - 300T_2 + 300T_1 - 137E] + \frac{\Delta^5}{6}u^{\text{VI}};$$

$$u'|_{r=R-\delta} = \frac{1}{60\Delta}[-10T_6 + 72T_5 -$$
$$-225T_4 + 400T_3 - 450T_2 + 360T_1 - 147E] + \frac{\Delta^6}{7}u^{\text{VII}}.$$

The main results of computation. The research computation was performed using the computing methods developed for experimental conditions (see Table 1) implemented in a one-diaphragm aerodynamic shock tube (at the Institute for Problem Mechanics, RAS) [8, 9]. During the experiments on the shock tube mentioned above, which were then subjected to the numerical analysis, at the initial instant of time (i.e., before the rupture of the diaphragm), the low pressure chamber (LP chamber) was filled with air (test gas) at pressure p_{LPc} [mbar] and temperature $T = 298.15$ K, while the high pressure chamber (HP chamber) was filled with a compressed air at pressure P_{HPc} [mbar] and temperature $T = 298.15$ K. The experimental facility at the Institute for Applied Mechanics, RAS, looks like a tube of an uniform cross-section (internal diameter $D = 0.8$ m; length of low pressure chamber $L_{LPc} = 7.35$ m; length of high pressure chamber $L_{HPc} = 1.97$ m) and is designed for the value range of Mach numbers SW $M = 6 \ldots 12$].

No	1	2	3	4	5	6	7	8	9	10	11
p_{HPc}, atm	10	10.2	22	19	13.2	19.5	19.5	20.5	21	36	34
p_{LPc}, atm	0.3	15	6.6	100	2	0.7	5.6	100	100	1	1

In Fig. 2, the layout chart of the pressure gauge locations used for obtaining the experimental time dependences of pressure $P(t)$ (in different spatial points) is shown.

In Fig. 3, the experimental (Experiment 4) time dependencies of pressure $P(t)$ for the second and third pressure gauges are shown (pressure gauge 1 is at the right end of the shock tube plane (the Institute of Problem Mechanics, RAS, see Fig. 2.)

From the graphs in Fig. 3, it follows that only gas-dynamic parameters can be evaluated (by the times of the shock wave arrivals to the pressure gauges) behind the front of the initial shock wave (gauge 2: $z = 5.78$ m, $t = 8.92$ ms; gauge 3: $z = 9.22$ m, $t = 14$ ms): $D_{\text{SW}} \approx 0.7$ km/s, $u_2 = \dfrac{2}{\gamma_1 + 1}D_{\text{SW}} \approx 0.6$ km/s, $p_2 = \dfrac{2}{\gamma_1 + 1}\rho_1 D_{\text{SW}}^2 \approx 0.5$ atm. From

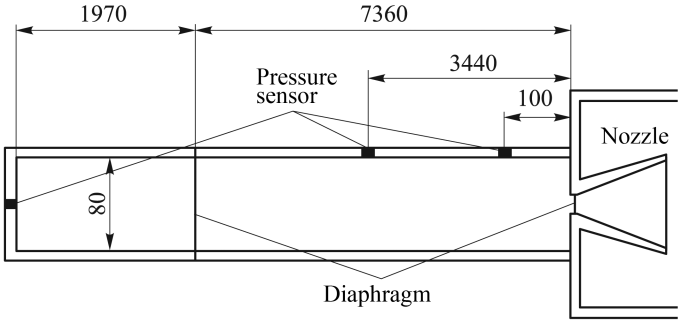

Fig. 2. The layout chart of pressure gauge locations in one-diaphragm shock tube (at the Institute for Problem Mechanics, RAS)

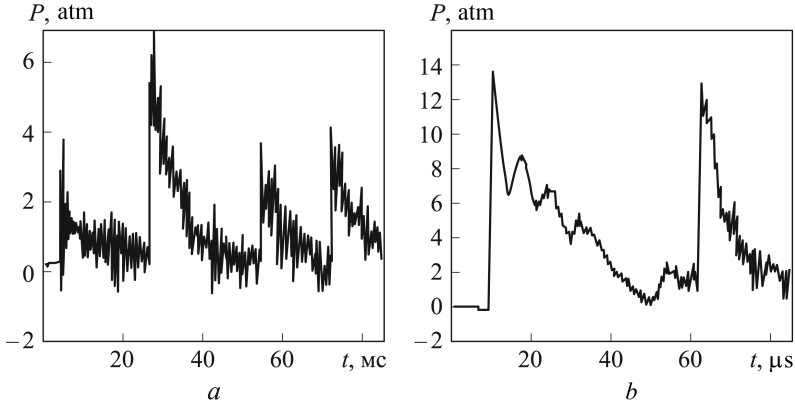

Fig. 3. Experimental time dependencies for the second (*a*) and third (*b*) pressure gauges (Experiment 4)

the graphic curve of pressure gauge 2 ($z = 5.78$ m), it follows that the observed maximum of the amplitude corresponds not to the initial shock wave arrival, i.e., not to the time $t \approx 9$ ms, but to a later instant $t \approx 30$ ms.

This phenomenon might be associated with the fact that at the moment of time $t \approx 30$ ms, at the point where gauge 2 is installed (approximately near the center of the computed area), the shock wave amplification after its reflection from the end surfaces of the shock tube is significantly higher that its attenuation during its interaction with rarefaction waves. These graphic curves also indicate that the further (relative to time) gas wave motion in a shock tube results in shock wave attenuation and the transition of the flow into the acoustic wave movement.

Thus, it may be noted that the unsteady gas flowing in the aerodynamic shock tube has a number of features which require a more detailed numerical study. The analysis of the characteristics of the flow in the shock tube of the Institute for Applied Mechanics, RAS, at the initial stage of study is preferably to be carried out using an approximate one-dimensional model, the elements of which are presented in this paper.

While developing an approximate one-dimensional model, a scheme of the computed area was used, as shown in Fig. 2. On the left side of the computed area there is a shock tube end wall for which a boundary condition was set, that of gas medium "non-leaking" through a solid barrier. On the right side of the integration field, the boundary condition of "non-leaking" was also stated. Thus, during the computation, it was approximately assumed that on the left side, the shock tube is limited by a solid wall (actually in this shock tube (at the Institute of Applied Mechanics, RAS, see Fig. 2), there is a Laval nozzle).

The resulting initial structure of the gas flow after the rupture of the diaphragm is shown in Fig. 4 and described in the notes. This structure of gas flow corresponds to the phase of wave system autonomic distribution in the space and extends for a time interval $0 \leqslant t \leqslant 0.85$ ms. As known [10], the shock wave intensity is accepted to be characterized with a dimensionless parameter called a shock wave amplitude: $Z = \dfrac{p_2 - p_1}{\rho_1 c_1^2}$. The levels of temperature and pressure values behind the shock wave front at this stage are specified by $T \approx 0.7$ кK, $p \approx 0.7$ atm. In the vicinity of the computed area boundaries, the gas is not disturbed and corresponds to the initial conditions (right boundary — $T = 298.15$ K, $p = 19$ atm; left boundary — $T = 298.15$ K, $p = 0.1$ atm). The following flow structure is observed for the time interval $0.85 \leqslant t \leqslant 10.3$ ms and is up to the phase of the initial interaction of shok waves and rarefaction waves with a solid barrier.

The result of shock wave reflection from the solid barrier that is located on the right of the area of integration is shown in Fig. 5. It is known that

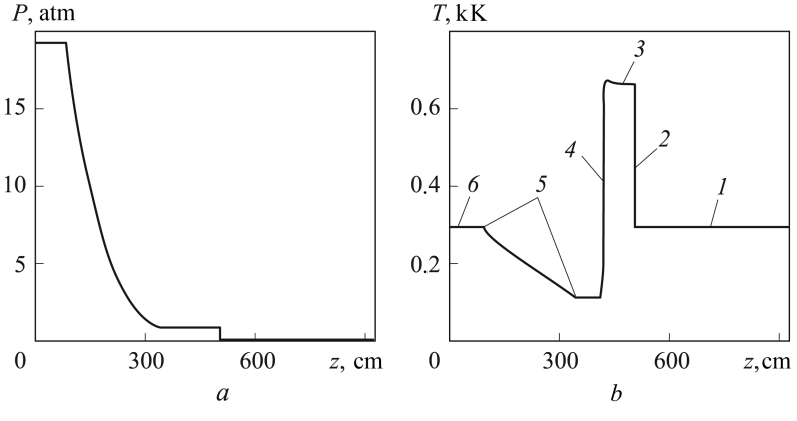

Fig. 4. Spatial distribution of pressure (*a*) and temperature (*b*) at the moment $t = 3.4$ ms after the rupture of the diaphragm (Experiment 4):
1 — unperturbed test (driven) gas; *2* — shock wave front; *3* — area of shock-compressed test (driven) gas; *4* — contact boundary front; *5* — space occupied by the rarefaction wave in the test (driven) gas; *6* — space corresponding to the initial state of the driver gas in the high pressure chamber

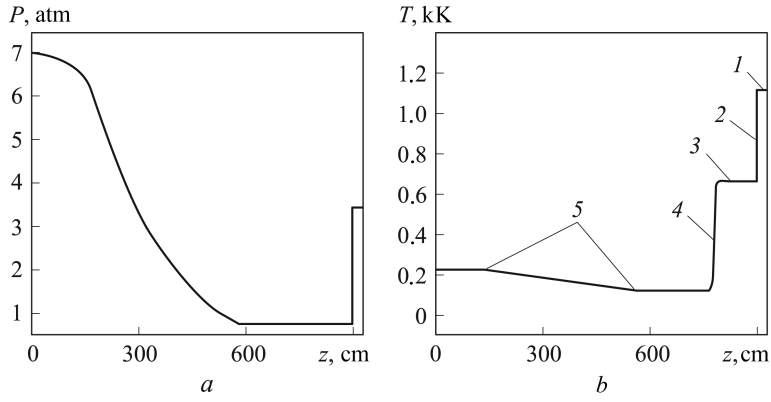

Fig. 5. Spatial distribution of pressure (*a*) and temperature (*b*) at the moment $t = 9.1$ ms (Experiment 4):
1 — shock-compressed test (driven) gas behind the reflected shock wave; *2* — reflected shock wave front; *3* — area of the initial shock-compressed test (driven) gas; *4* — contact boundary front; *5* — space occupied by the rarefaction wave in driver gas

the most significant peculiarity of the interaction of a shock wave with a solid barrier is the shock wave amplification after its reflection from the barrier [10]. It is convenient to characterize the process of the shock wave reflection by the relative amplification coefficient: $K = \dfrac{\Delta p_3}{\Delta p_2}$, where $\Delta p_3 = p_3 - p_1$ is the excessive pressure in the reflected shock wave, $\Delta p_2 = p_2 - p_1$ is the excessive pressure in the incident wave.

From graphic curves given in Fig. 3, it follows that the shock wave collision with the solid barrier results in the appreciable amplification of the reflected shock wave: the amplification coefficient $K \approx 6$ (for air the maximum value of amplification coefficient is $K = 8$). The amplitude value of the reflected shock wave $Z \approx 24$, the temperature and pressure at the right computed boundary increase to $T \approx 1.2$ кК, $p \approx 3.5$ atm. By this moment, the fan-shaped flow of rarefaction waves has already reflected from the left computed boundary and moved more than half into the computed zone. Along with it, the temperature and pressure at the left boundary have dropped to $T \approx 0.2$ кК, $p \approx 7$ atm.

Then, mostly at the right computed boundary, we can observe the flow structure (Fig. 6) corresponding to the phase of complex interaction of the shock wave, contact discontinuity, and rarefaction wave, which expands approximately for $10.3 \leqslant t \leqslant 10.3 + \dfrac{L_{HPc} + L_{LPc}}{c_1} \approx 35$ ms. The reflected shock wave interacts only with the contact discontinuity that moves towards it at the initial stage of the phase of flowing in the shock tube in the vicinity of the right computed boundary.

In this case there can be two options of the interaction: a) if the shock wave interacting with the contact discontinuity expands from the denser

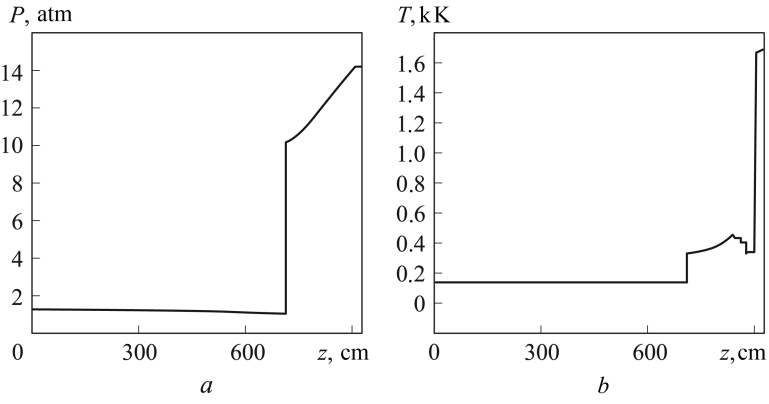

Fig. 6. Spatial distribution of pressure (*a*) and temperature (*b*) at the moment $t = 3.4$ ms (experiment 4)

medium into the less dense medium, then it will reflect from the contact discontinuity in the form of a fan of rarefaction waves; b) if the case is opposite – from the less dense medium into the denser one, - then the reflection takes the form of a shock wave.

In the numerical computation done, the interaction type (a) has been implemented, and the fan of rarefaction waves has been repeatedly reflected from the shock tube wall and from the contact discontinuity. A bit later the process of waves interaction is becoming more complicated, which results from the influence of the reflected from the left boundary rarefaction wave. Along with this, the temperature and pressure at the left boundary have been equalized and reduced their values as compared to the previous phase of flowing $T \approx 0.15$ кК, $p \approx 1.5$ atm.

The following flow structure (see Fig. 7) can be observed starting since the moment of time 35 ms and it corresponds to the phase of the secondary interaction of the shock wave reflected from the left computed boundary

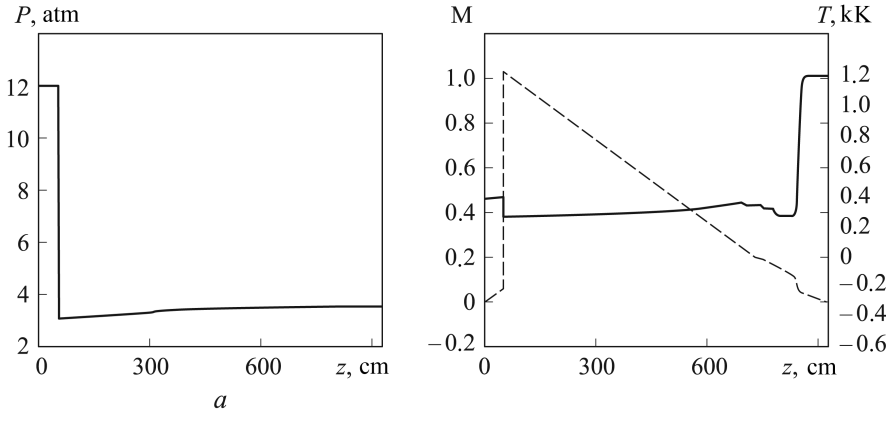

Fig. 7. Spatial distribution of pressure (*a*), Mach number M (*b*) (dashed line), temperature (solid line) at the moment $t = 42$ ms (Experiment 4)

(solid barrier). The following curves show that the gas wave flow in the shock tube results in a relatively weak shock wave attennuation. The values of the reflected shock wave amplitude and the pressure in the vicinity of the left boundary are on a relatively high leve l$z \approx 80$, $p \approx 12$ atm, but the temperature has dropped to $T \approx 0.4$ кK. By this moment of time, in the most part of the computed zone, the pressure and temperature have almost similar values $T \approx 0.4$ кK, $P \approx 3.5$ atm, but they are quite high in comparison with the initial conditions in the low pressure chamber. It can be explained by the active processes of relaxation occurring in the shock tube. It is interesting that if the processes of equalization in the shock tube had completely come to an end, then the values of termodynamic parameters $T \approx 0.12$ кK, $p \approx 1.63$ atm would have been set.

It should be noted, that the proposed computational algorithm, which is intended for numerical modeling of aerothermophysical characteristics of the aerodynamic shock tubes, is to be compared with the published computational and experimental results.

For this purpose, experimental and computational time dependences obtained for pressure gauges 2 and 3 were compared (Fig. 8). From the graphs of the experimental dependences (it 1, it 2) it follows that the first period of pressure $P(t)$ change (and for gauge 2 — both the first and the second periods) differ noticeably from the following periods. This difference might be caused by the "transition" processes (which can be caused by the gas outflowing through the Laval nozzle and various factors distorting the one-dimensional flow pattern in the shock tube) occurring

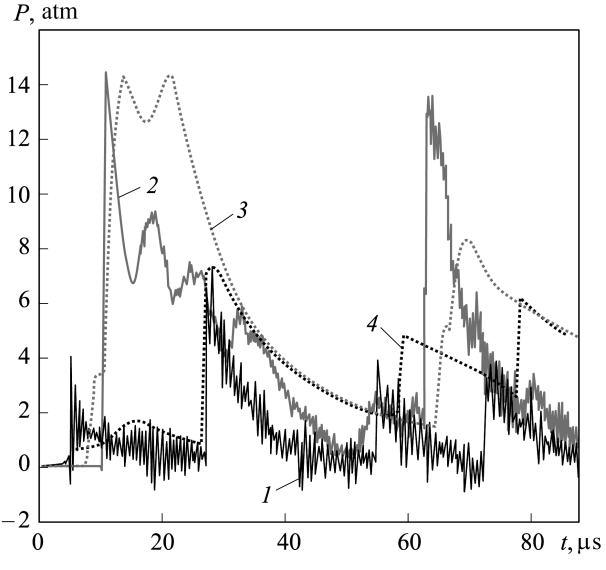

Fig. 8. Experimental (*1* and *2*) and computational (*3* and *4*) time dependences for the second (*1* and *4*) and third (*2* and *3*) pressure gauges (Experiment 4) (dashed line — computation; solid line — experiment)

in the shock tube at the initial stage. The comparison of experimental and computational physical dependences (see Fig 8) allows noting satisfactory coincidence between them.

Conclusion. The numerical methods and the computation code for non-stationary one-dimensional radiation magnetogasdynamic models are developed, which are intended to describe the thermophysical processes in various types of shock tubes. The numerical solution of the non-stationary radiation magnetogasdynamic model described in this article is based on the splitting method according to the physical processes and spatial directions. The solution of the splitted equations is to be found using the developed non-linear quasimonotonous compact difference scheme of the higher order of accuracy, which allows achieving the seventh order of accuracy in the spatial smooth part of the numerical solution. The proposed mathematical apparatus can be used for solving more complicated Reynolds equations. The solution to the formulated problem will enhance the further experimental and theoretical research into the shock tubes.

The work has been fulfilled in the Laboratory for Radiation Gas Dynamics at Ishlinskii Institute for Problems in Mechanics of the Russian Academy of Science (RAS) within the programme of RAS Fundamental Research.

REFERENCES

[1] Riddell F.R. Study of hypersonic flows. New York-London, Acad. press, 1962. 513 p. (Russ. ed.: Issledovanie giperzvukovykh techenii. Sb. statei pod red. F.R. Riddella. Moscow, Mir Publ., 1964. 544 p.).

[2] Kovenia V.M., Yanenko N.N. Metod raschepleniia v zadachakh gazovoi dinamiki [Splitting method in gas dynamics problems]. Moscow, Nauka Publ., 1981. 304 p.

[3] Volkov K.N., Emelianov V.N. Modelirovanie krupnykh vikhrei v raschetakh turbulentnykh techenii [Large eddy simulation (LES) for the turbulent flow calculations]. Moscow, Fizmatlit Publ., 2008. 364 p.

[4] Marchuk G.I., Shaidurov V.V. Povyshenie tochnosti resheniia raznostnykh skhem [The improvment of difference scheme solution accuracy]. Moscow, Nauka Publ., 1979. 320 p.

[5] Dovgilovich L.E., Sofronov I.L. O primenenii kompaktnykh skhem dlia resheniia volnovogo uravneniia [On application of compact schemes for solving wave equations]. Moscow, Preprint No. 84 of Keldysh Institute of Applied Mathematics, IPM im. M.V. Keldysha Publ., 2008. 27 p. URL: http://library.keldysh.ru/preprint.asp?id=2008-84 (accessed 30.08.2013).

[6] Barth T.J. On unstructured grids and solvers in Computational Fluid Dynamics. Belgium, The von Karman Institute for Fluid Dynamics, 1990, Lecture Notes Series 1990-04.

[7] Saveliev A.D. Sostavnyie kompaktnyie skhemy vysokogo poriadka dlia modelirovaniia techeniia viazkogo gaza [High-order composite compact schemes for simulation of viscous gas flows. *Zhurnal vychislitel'noi matematiki i matematicheskoi fiziki* [J. of Computational Mathematics and Mathematical Physics], 2007, vol. 47, No. 8, pp. 1387–1401 (in Russ.).

[8] Kotov M.A., Kuzenov V.V. Obzornyi analiz eksperimental'nykh issledovanii, vypolnennykh s pomoshch'iu nekotorykh tipov udarnykh trub. [A review of experimental investigations performed using some types of shock tubes]. Moscow, Preprint no. 1044 of RAS Appl. Mech. Inst., IPMech RAN Publ., 2013. 75 p.

[9] Kotov M.A., Kryukov I.A., Ruleva L.B., Solodovnikov S.I., Surzhikov S.T. Experimental Investigation Of An Aerodynamic Flow Of Geometrical Models In Hypersonic Aerodynamic Shock Tube. *Proc. AIAA Wind Tunnel and Flight Testing Aero II*, San Diego, June 24–27, 2013, no. 2013-2931. URL: http://arc.aiaa.org/doi/abs/10.2514/6.2013-2931(accessed 30.08.2013).

[10] Ovsiannikov L.V. Lektsii po osnovam gazovoi dinamiki [Lectures on the fundamentals of gas dynamics]. Moscow, Nauka, Publ., 1981. 368 p.

The original manuscript was received by the editors in 30.08.2013

Contributors

Kuzenov V.V. — Ph.D. (Eng.), Associate Professor of Engineering, Senior Research Fellow, Laboratory for Radiation Gas Dynamics, Ishlinskii Institute for Problems in Mechanics of the Russian Academy of Sciences, author of over 110 research publications in the fields of thermal physics and radiation gas dynamics.
Ishlinskii Institute for Problems in Mechanics of the Russian Academy of Sciences, Vernadskogo prospekt 101, Moscow, 119526 Russian Federation.

Kotov M.A. — laboratory scientist, Laboratory for Radiation Gas Dynamics, Ishlinskii Institute for Problems in Mechanics of the Russian Academy of Sciences, author of over 15 research publications in the field of aerothermophysics.
Ishlinskii Institute for Problems in Mechanics of the Russian Academy of Sciences, Vernadskogo prospekt 101, Moscow, 119526 Russian Federation.

The translation of this article from Russian into English is done by O.G. Rumyantseva, a senior lecturer in the Chair of English Language, Linguistics Department, Bauman Moscow State Technical University under the general editorship of N.N. Nikolaeva, Ph.D. (Philol.), Associate Professor in the Chair of English Language, Linguistics Department, Bauman Moscow State Technical University.